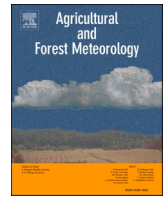


Contents lists available at [ScienceDirect](https://www.sciencedirect.com)

Agricultural and Forest Meteorology

journal homepage: www.elsevier.com/locate/agrformet

Atmospheric jet stream variability reflects vegetation activity in Europe

Gabriele Messori^{a,b,c,1,*}, Minchao Wu^{a,1}, Giulia Vico^d, Vera Melinda Galfi^a

^a Department of Earth Sciences, Uppsala University, Villavägen 16, Uppsala 752 36, Sweden

^b Centre of Natural Hazards and Disaster Science (CNDS), Uppsala University, Uppsala, Sweden

^c Department of Meteorology and Bolin Centre for Climate Research, Stockholm University, Stockholm, Sweden

^d Department of Crop Production Ecology, Swedish University of Agricultural Sciences (SLU), Uppsala, Sweden

ARTICLE INFO

Keywords:
Jet Stream
Vegetation
Europe
EVI2

ABSTRACT

Jet streams are a key component of the climate system, whose dynamics couple closely to regional climate variability. Yet, the link between jet stream variability and vegetation activity has received little attention. Here, we leverage our understanding of the mid-latitude jet stream dynamics over the Euro-Atlantic sector to probe climate–vegetation interactions across Europe. We link indices related to the meridional location of the jet and the large-scale zonal wind speed with remotely-sensed vegetation greenness anomalies during locally-defined growing seasons. Correlations between greenness anomalies and jet latitude anomalies point to a control of the jet stream's variability on vegetation activity over large parts of Europe. This potential control is mediated by the jet latitude anomalies' correlations with temperature, soil moisture and downward surface solar radiation. The sign and strength of these correlations depend on location and time of the year. Furthermore, jet stream variability modulates conditions at the onset and end of the growing season. The link between jet latitude anomalies and vegetation greenness is not only specific to the climate zone, but also to the landclass and sub-period within the growing season. It is thus important to use a locally-defined growing season for interpreting the atmospheric controls on regional vegetation phenology. Results consistent with the correlation analysis emerge when focussing on local high or low greenness months only or on zonal wind speed anomalies, confirming the relevance of jet variability for vegetation activity.

1. Introduction

Climate and vegetation dynamically interact across a range of timescales, from sub-daily to seasonal, interannual and longer (e.g. Urbanski et al., 2007; Rödenbeck et al., 2018; Messori et al., 2019 and Refs. therein; Bastos et al., 2021). Notably, ongoing climate change has already had measurable impacts on global greenness and vegetation activity (e.g. Zhu et al., 2016; Menzel et al., 2020), and future climate change may enhance regional vegetation–climate feedbacks (e.g. Wu et al., 2021a). Links between climate and the terrestrial carbon cycle are active year-round (e.g. Wang et al., 2011), but the direct effects of climate on vegetation activity occur primarily during the growing season (GS), whose timing depends on local climatic conditions and vegetation type (Wu et al., 2021b). The control of climatic conditions on vegetation is often expressed in terms of local downward surface solar radiation, temperature, soil moisture, and their combinations. The relative importance of these different factors depends on the background

climatic conditions themselves, as well as vegetation type and subperiod of the GS. In turn, vegetation can affect local and regional climate, for example through its role in land–atmosphere coupling (Williams and Torn, 2015), and by modulating surface air temperature (Wu et al., 2017; Zeng et al., 2017) and hydroclimate (Jiang et al., 2015). This two-way interaction can lead to complex land–atmosphere feedback loops, in which vegetation plays a key role (Zeng and Neelin, 2000; Meng et al., 2014; Zeng et al., 2017). Nonetheless, climatic controls on vegetation are typically considered the first-order effect on regional and larger spatial scales, at least in the present-day climate and extratropical region (e.g. Messori et al., 2019, and references therein).

Here, we focus on the potential impact of climate variability on vegetation activity. Making this complex link amenable to analysis requires developing a low-dimensional representation of the high-dimensional, chaotic spatio-temporal climatic variability. A first step is typically to focus on the atmosphere. Other components of the climate system (e.g., the ocean) act on timescales longer than those typical of

* Corresponding author at: Department of Earth Sciences, Uppsala University, Villavägen 16, Uppsala 752 36, Sweden.

E-mail address: gabriele.messori@geo.uu.se (G. Messori).

¹ These authors have contributed equally to the work.

<https://doi.org/10.1016/j.agrformet.2022.109008>

Received 17 October 2021; Received in revised form 7 April 2022; Accepted 14 May 2022

Available online 26 May 2022

0168-1923/© 2022 The Author(s). Published by Elsevier B.V. This is an open access article under the CC BY license (<http://creativecommons.org/licenses/by/4.0/>).

vegetation responses, and their impact on vegetation is chiefly mediated by the atmosphere (for an example relative to ENSO, see Jones et al., 2001). A second step is to consider individual atmospheric variables, such as temperature or precipitation (e.g. Wang et al., 2003) or multivariate indicators, such as drought indices (e.g. Gouveia et al., 2017). Alternatively the atmospheric variability is collapsed into a small number of reference states, which are typically linked to climate modes of variability (e.g., ENSO or the North Atlantic Oscillation; Bjerknes, 1969, Hurrell and Visbeck, 2001) and the associated teleconnection indices (Glantz, 1991). These indices have been used to explore the climatic controls on vegetation activity. For example, Gouveia et al. (2008) found strong evidence that the winter North Atlantic Oscillation modulates vegetation activity during the subsequent spring and summer in different parts of Europe, owing to the control it exerts on wintertime precipitation and temperatures. In a later study, Gonsamo et al. (2016) argued for wide-ranging impacts of different climate modes of variability on vegetation activity, primarily through their influence on temperature. Notwithstanding this, climate modes of variability only reflect a limited portion of the full atmospheric variability, and may be difficult to relate to the underlying physical drivers (Dommenget and Latif, 2002).

To further advance our understanding of climate–vegetation interactions, there is the need for climate indices that share the immediacy of conventional teleconnection indices, while maintaining a direct link to the dynamical processes governing atmospheric variability. Indices that reflect the characteristics of the mid-latitude atmospheric jet stream provide a complementary aggregation of information on climate variability compared to climate modes, and offer a promising way forward. Indeed, the jet streams relate to the basic physical principles governing the large-scale atmospheric circulation (e.g. Rossby, 1947, Held, 1975, Held and Hou, 1980), which may be conceptualised as arising from the interplay between the mean meridional circulation, mid-latitude jet streams and baroclinically unstable eddies. Jets also couple closely to regional climate variability and extreme events (e.g. Gaetani et al., 2011, Santos et al., 2013, Röthlisberger et al., 2016, Messori et al., 2016). Finally, jet stream variability can be linked back to the climate mode of variability paradigm, as anomalies in the jet reflect the positive or negative phases of a number of climate modes (e.g. Woollings et al., 2010, Messori and Caballero, 2015, Parker et al., 2019).

Jet stream indices thus have the potential to provide valuable insights into climate–vegetation interactions, yet their use in this context has been thus far limited, and the relations between jet stream variability and key drivers of vegetation activity have not been systematically explored. Belmecheri et al. (2017) provided a cogent proof-of-concept for the applicability of jet indices to the study of vegetation and carbon cycle variability, and Hudson et al. (2019) leveraged the jet stream as a tool to understand tree growth variability in the Northern Rocky Mountains in the United States of America. Both studies have focussed on the North American continent when looking at climate–vegetation interactions, although Belmecheri et al. (2017) also proposed a hemispheric-scale jet index. The links between the jet stream and vegetation activity remain unexplored in Europe.

When focussing on Europe, the mid-latitude jet over the Euro-Atlantic sector is of particular interest. Several indices have been proposed to diagnose its location and characteristics (e.g. Woollings et al., 2010, Harnik et al., 2014, Messori and Caballero, 2015, Molnos et al., 2017, Faranda et al., 2019, Messori et al., 2021). Here, we use the Jet Latitude Index (JLI) and Zonal Speed Index (ZSI). The former identifies anomalies in the meridional location of the jet, while the latter reflects anomalies in the mean zonal windspeed across the North Atlantic and Europe at a given latitude. The ZSI thus complements the JLI, by providing large-scale flow information also at latitudes that do not correspond to that of the jet. We explore the correlation between these two indices and vegetation activity across Europe, based on the two-band Enhanced Vegetation Index (EVI2). We focus on a locally-defined GS, which we argue is key for interpreting the

atmospheric controls on regional vegetation activity. We hypothesize that the JLI and ZSI explain anomalies in vegetation activity, through the location-specific relations between them and key vegetation drivers. Further, we test whether the JLI modulates the local GS onset and end. This illustrates the insights that jet and zonal flow indices can afford in the context of climate–vegetation interactions.

2. Data and methods

2.1. Data

To compute the jet and zonal flow indices, we use the 6 h zonal component of the wind at 300 hPa for the period 1981–2019 from ECMWF's ERA5 reanalysis data set (Hersbach et al., 2020), with a horizontal resolution of 0.5° . The effects of different jet stream configurations on the climate in Europe are diagnosed using monthly-averaged 2m air temperature (hereafter referred to simply as *temperature*) and total precipitation from the same reanalysis dataset at the same spatial resolution. The total precipitation represents the sum of large-scale and convective precipitation, with a 1-day accumulation period.

The variability of vegetation activity over Europe was inferred from EVI2 data (Jiang et al., 2008), derived from the multi-sensor Vegetation Index and Phenology satellite product. EVI2 improves vegetation signal sensitivity for high-biomass ecosystems relative to the Normalized Difference Vegetation Index, while minimising the confounding influence of soil and atmospheric conditions, including aerosols, on said signal (Jiang et al., 2008). It provides one of the longest available continuous records of satellite-based vegetation index (1981/01–2014/12) at bi-weekly and 0.05° resolutions.

A number of additional datasets were used to investigate the local climate–vegetation coupling, including downwards surface solar radiation (hereafter simply *radiation*) from ERA5 (Hersbach et al., 2020), and root-zone soil moisture from the Global Land Evaporation Amsterdam Model (GLEAM, Miralles et al., 2011; Martens et al., 2017). These data sets have monthly temporal and 0.25° spatial resolution. The 0.5° monthly frost day frequency from CRU TS404 (Harris et al., 2020) was used to define the local GS in combination with the vegetation phenology. The 0.05° MODIS IGBP landclass data set MCD12C1 (Friedl et al., 2010) and the 0.5° Köppen–Geiger climate classification (Kottek et al., 2006) were used to partition the data according to climate zone and land-cover type. Specifically, we consider eight land-cover types (EF: evergreen forest; DF: deciduous forest; MF: mixed forest; WS: closed shrubland, open shrubland, and woody savanna; GRS: grassland and savanna; CRP: crop land and natural vegetation mosaic; SIB: for snow, ice, barren soil, and sparse vegetation; Fig. S1a) and seven zones grouped according to climate and location (two Mediterranean, two Boreal and three Temperate zones; Fig. S1b). All the datasets were harmonized at monthly and 0.5° resolutions for the analysis, following Wu et al. (2021b). The temporal resampling was conducted by calculating mean values. The spatial resampling used a bilinear approach. For the landclass data, each 0.5° gridbox was assigned the landclass covering the largest areal fraction.

2.2. Methods

2.2.1. Jet and zonal flow indices

We consider two indices computed over the North Atlantic and Europe: the Jet Latitude Index, JLI, quantifying anomalies in the meridional location of the jet, and the Zonal Speed Index, ZSI, quantifying anomalies in the mean zonal windspeed at a given latitude.

To determine the JLI, we build upon the approach of Woollings et al. (2010). We compute the daily, zonal-mean zonal wind at 300 hPa at each latitude in the region 75° W– 50° E and 10° – 80° N, representing the North Atlantic and Europe. The latitude of the maximum zonal-mean zonal wind is taken as the jet's latitude. The mean maximum wind-speeds range from 33.9 m s^{-1} during December–January–February (DJF)

to 22.5 m s^{-1} during June–July–August (JJA), with the corresponding standard deviations being 5.1 and 4.0 m s^{-1} . Next, a jet latitude seasonal cycle is computed as the average daily jet latitude over all years in the dataset, smoothed with a 30-days running mean window. The JLI is then obtained as the daily deviation of the jet latitude from its seasonal cycle, aggregated on a monthly scale.

The ZSI for a given latitude in the range 10° – 80° N, is defined based on the zonal-mean zonal wind at 300 hPa over the region 75° W– 50° E. Similar to the JLI, the ZSI is computed as the deviation of the zonal-mean zonal wind from its seasonal cycle on a daily basis, and then aggregated on a monthly scale.

2.2.2. Locally-defined growing season

We use a locally-defined GS averaged over all years in our data, to capture the key periods for vegetation activity (Fig. S2). Following Wu et al. (2021b), the start of season is defined as the first month after the yearly minimum EVI2 when vegetation greenness is increasing, reaches at least 15% of the effective greenness (the difference between the maximum and minimum greenness within a seasonal cycle) and more than 15 days are frost-free. Similarly, end of season is the last month after the start of season with greenness decreasing yet remaining above 15% of the effective greenness and more than 15 frost-free days. The peak of season is defined as the average of the months with greenness attaining at least 85% of effective greenness. This allows splitting the GS in two subperiods: early GS, i.e. the period between start of season and peak of season; and late GS, i.e. the period between peak of season and end of season. When we instead refer to meteorological seasons, we equate summer with JJA, autumn with September–October–November (SON), winter with DJF and spring with March–April–May (MAM).

2.2.3. Assessment of the climate–vegetation coupling

To quantify the climate–vegetation coupling, we compute vegetation and climate anomalies and their correlations. The former anomalies are based on EVI2; the latter anomalies on both the climate variables described in Sect. 2.1 and the jet and zonal flow indices (Sect. 2.2.1). Both vegetation and surface climate data are deseasonalised using the monthly local seasonal cycle (i.e. the long-term mean of monthly or 30-day values), and detrended. Unless otherwise stated, statistical significance is evaluated using a 1-sample Student's t-test. Hereafter, we refer to the correlation between the EVI2 anomalies and JLI as *EVI2–JLI correlation*. In the case of a GS subperiod spanning several months (e.g. early GS or late GS), the correlation is computed using the mean values of the relevant variables throughout that subperiod. Both simultaneous (lag 0) and asynchronous climate–vegetation couplings are analysed. For example, for the case of a region with early GS in May and June, the

lag 0 analysis relates average vegetation anomalies in May and June to average climate anomalies during the same months. The asynchronous analysis at lag -1 months relates average vegetation anomalies in May and June to average climate anomalies in April and May.

3. Jet variability and vegetation activity in Europe

3.1. The jet as a dynamical control of vegetation activity

Jet stream variability is closely related to GS conditions over large parts of Europe. EVI2–JLI correlations are generally positive in boreal Fennoscandia, but negative elsewhere, with rare and mostly non-significant exceptions (Fig. 1). Extended regions of significantly negative correlations are largely limited to boreal eastern Europe, while Temperate and Mediterranean regions display weaker correlations with a noisy spatial pattern. As discussed below, the sign and strength of the correlations are mediated by canonical vegetation controls such as soil moisture, radiation and temperature over broad swaths of the continent.

Since Europe spans a number of different climate zones and land-classes (Fig. S1a, b), there is a large geographical variation in the relative importance of soil moisture, radiation and temperature as controls of vegetation during the GS and its subperiods. In many regions it is difficult to point to which of these three drivers is most important, in particular for the entire GS (Fig. S1c). Indeed, different drivers are often relevant for different GS subperiods (cf. Fig. S1d, e). In the entire GS, soil moisture is the dominant control in the Iberian Peninsula and parts of central Europe, while temperature or radiation are more important at higher latitudes and/or altitudes (e.g., central and northern Fennoscandia, parts of the Carpathians; Fig. S1c). This reflects the factors limiting vegetation growth, canonically water in southern Europe and energy in Northern Europe or at high-altitude locations. In the early GS, temperature and radiation are the key drivers across most of the continent except Iberia (Fig. S1d), whereas in the late GS soil moisture dominates in central and southern Europe and radiation in northern Europe (Fig. S1e).

JLI correlates significantly with temperature, soil moisture and radiation anomalies regionally, but the sign and strength of these correlations depend on location and season (Figs. 2a, d, g and S3a–l). This may largely be ascribed to the seasonality of atmospheric dynamics, such as differences in the average meridional location of the jet and the different characteristics of both oceanic and continental air masses throughout the year. The different landclasses dominating the different latitudes may also play a role, although this would be hard to isolate. By virtue of the large specific heat capacity of water, in the warmer months the moist oceanic air is generally cooler than the continental airmasses,

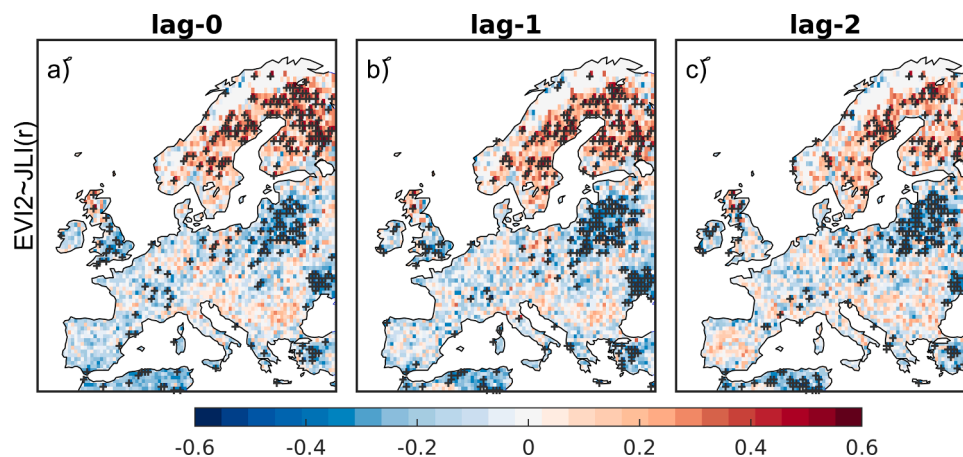


Fig. 1. GS EVI2–JLI correlation coefficients at lags of 0, -1 and -2 months (where at negative lags the signal in the JLI timeseries precedes the signal in the EVI2 anomaly timeseries). Gridpoints with a significant correlation coefficient ($p < 0.05$) are stippled. In all figures, unless otherwise specified, white indicates no data, no GS due to invalid data points, or (near-) zero correlation.

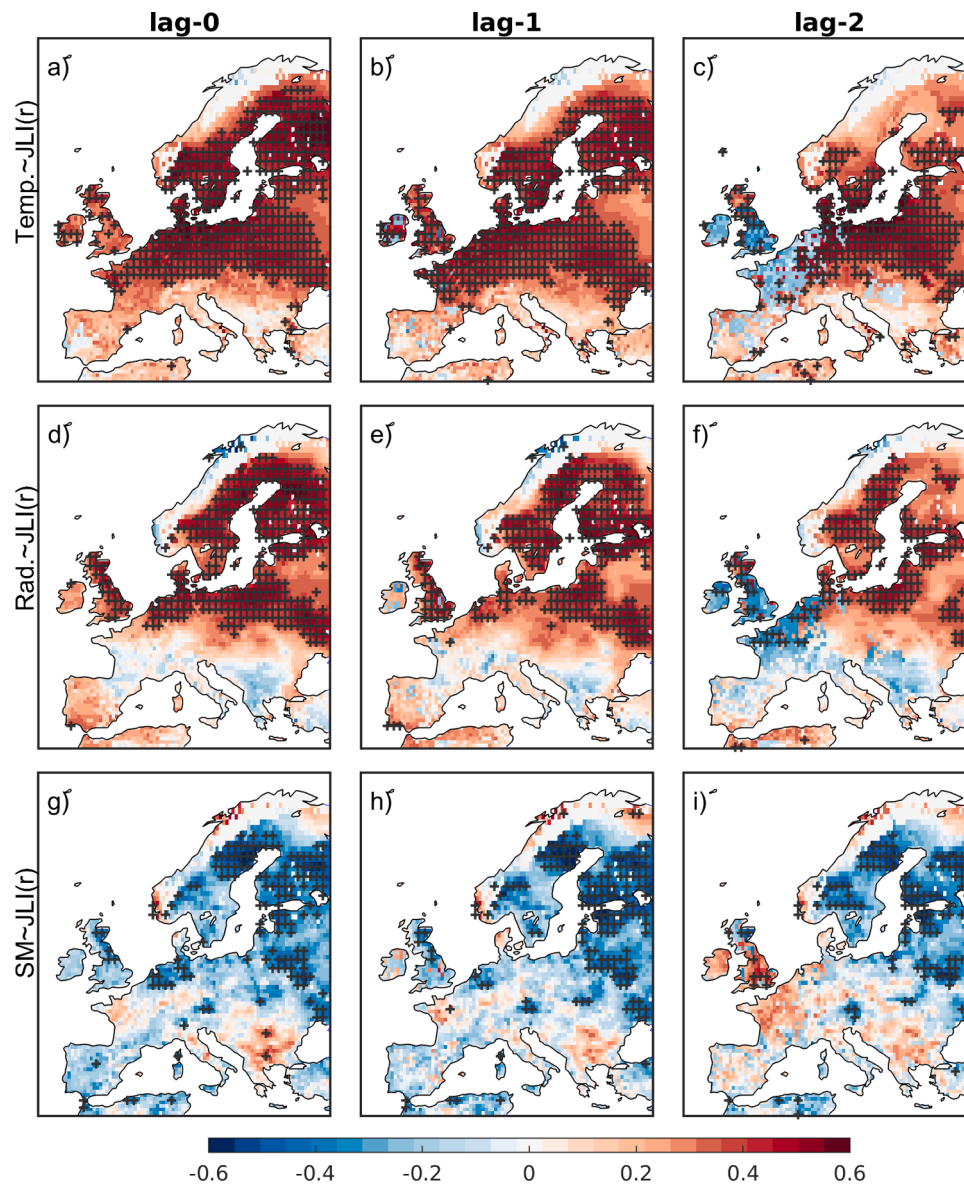


Fig. 2. GS correlation coefficients of temperature (Temp., a–c), radiation (Rad., d–f) and soil moisture (SM, g–i) anomalies with JLI at lags of 0, -1 and -2 months (where at negative lags the signal in the JLI timeseries precedes the signal in the Temp., Rad., or SM anomaly timeseries). Gridpoints with a significant correlation coefficient ($p < 0.05$) are stippled.

whereas the opposite holds in winter. Thus, the implications of a strengthened or weakened westerly flow also change. The correlation of JLI with temperature anomalies during the GS is generally positive and significant over the northern half of the continent, and weakens to the south (Fig. 2a). GS months when the jet stream lies to the north of its climatological position thus correspond to warmer temperatures in the north, and *vice-versa* for southward shifts. The implications of a northward shift of the jet in terms of atmospheric dynamics are particularly evident during summer, when the jet is climatologically further north than in winter (e.g. Woollings et al., 2014). A northward shift implies that the jet is to the north of much of Europe and indeed positive JLI events show a weaker than usual zonal flow over continental Europe (Fig. S4b). Fig. S4b additionally shows a jet stream core ending in the middle North Atlantic, suggesting a blocked atmospheric flow, or more broadly a weakening and/or distortion of the climatological westerly flow in the North Atlantic. Such a flow limits the influx of comparatively cool oceanic airmasses over the continent. A negative JLI has the opposite effect, corresponding to enhanced zonal advection of oceanic airmasses over the continent (cf. Fig. S4b, f).

Consistently with this picture of the atmospheric dynamics, we see a positive correlation between temperature anomalies and JLI during JJA over much of continental-northern Europe, the British Isles and Fennoscandia (Fig. S3b). Composite anomalies, conditioned on large or small JLI values, further highlight that a northward-shifted jet during JJA corresponds to moderate positive temperature anomalies over the same regions and months, when compared to a southward-shifted jet (Fig. S5b). Since the GS in northern Europe and Fennoscandia generally spans the whole summer period (Fig. S2), the correlation pattern in Fig. 2a is fully consistent with these jet-mediated circulation anomalies. The spatial pattern of simultaneous correlation of JLI with radiation anomalies (Fig. 2d) follows relatively closely that of temperature and further supports our dynamical interpretation. During summer, warm spells and a weakened influx of moist oceanic air over northern Europe are typically associated with clear skies, and hence enhanced solar radiation reaching the surface (see also Fig. S3f).

In contrast to radiation, soil moisture anomalies and JLI are significantly negatively correlated in northern Europe, Fennoscandia and the British Isles (Fig. 2g). Hence, soils are dryer (wetter) there when the jet is

shifted northwards (southwards). This is in line with a northward-shifted jet in summer corresponding to a diversion and/or weakening of the climatological westerly advection of moist oceanic air towards the continent, and leading to warmer temperatures and higher levels of radiation (see also Fig. S3j). A southward-shifted jet in summer effects the opposite result. Indeed, positive JLI values during JJA correspond to decreased precipitation over much of the British Isles and northern Europe when compared to negative JLI values (Fig. S5f).

We ascribe the generally non-significant correlations shown in Fig. 2 across the Mediterranean basin and southern Europe to the very long GS in these regions, which conflates months displaying radically different meteorological characteristics. Indeed temperature, and to a lesser extent radiation and soil moisture anomalies, show correlations of opposite signs with the JLI depending on the meteorological season (Fig. S3). Analysing correlations for data aggregated over GS subperiods may provide additional information in this context.

The correlation analysis between JLI and GS conditions at lags of -1 and -2 months, i.e., for the signal in the JLI timeseries preceding the signal in the soil moisture, temperature or radiation anomaly timeseries (Fig. 2b, c, e, f, h, i), provides results similar to lag 0. The exceptions are the southern British Isles and northern France/Benelux, where the correlations with temperature and radiation anomalies decrease with lag from moderately positive to moderately negative, while that with soil moisture displays the opposite shift. These regions display a start of season in early spring (Fig. S2a), and thus lag -2 includes JLI values for late winter. During late winter, there is a positive correlation between JLI and soil moisture anomalies and a negative correlation between JLI and radiation anomalies in the southern British Isles and northern France/Benelux (not shown). Indeed, the jet is climatologically further south than in summer, meaning that a northward (southward) jet excursion in that season does not necessarily imply a weakened (strengthened) advection of moist oceanic air over these regions. The JLI–soil moisture link during late winter may in turn modulate the conditions in the early part of the GS.

The observed correlations between JLI and EVI2 anomalies can be explained by the control of the jet stream on GS conditions across the continent. For example, the positive correlations in boreal Fennoscandia are likely mediated by local early GS temperature (Fig. S1d; Fig. S6a, Fig. S7a). In this region GS are short (Fig. S2d), and the timing of suitable thermal conditions and the occurrence of damaging spring frost control plant activity during the early GS (Marquis et al., 2020; Muffler et al., 2016). Indeed, the correlation between JLI and EVI2 anomalies is strongest in the early GS (see Sect. 3.2). Boreal eastern Europe, despite also belonging to the boreal domain, displays primarily negative EVI2–JLI correlations (Fig. 1). This likely reflects the role of multiple factors, including soil moisture anomalies which are negatively correlated with the JLI in the region (Fig. 2g), and radiation anomalies (Fig. S1c). The former are of particular importance during the late GS (Fig. S1e), when they correlate positively with EVI2 anomalies (Fig. S7f), promoting an overall negative EVI2–JLI correlation. The persistence of soil moisture may explain the strong negative correlation found in the area for lag -2, which would then relate soil moisture during the peak GS to vegetation greenness in the late GS (Fig. 1c). Radiation anomalies are instead of particular importance during the early GS (Fig. S1d) and are positively correlated with JLI yet negatively or neutrally correlated with EVI2 anomalies over much of Boreal eastern Europe (Fig. S7c), consistent with a negative EVI2–JLI correlation. We speculate that high radiation correlates with large diurnal temperature ranges, such that vegetation receives a high radiation input at sub-optimal temperatures for photosynthesis and suffers photooxidative damage (e.g., Öquist and Huner, 2003). The relative importance of soil moisture and radiation varies across boreal eastern Europe, with radiation dominating in the southern portion of the region (Fig. S1c).

Jet anomalies also modulate the start and end of season conditions at multiple lags. At the start of season, eastern Fennoscandia, central-western, southern and south-eastern Europe show geographically

coherent regions of significant positive EVI2–JLI correlations (Fig. 3a). These are also reflected in the correlations aggregated by climate zone and landclass, with the majority of landclasses in Boreal Fennoscandia, the three temperate climates and the central-eastern Mediterranean displaying significant positive correlations (Fig. S8a, c–e, g). Significant negative correlations are instead found in eastern Europe and the southern part of the British Isles (Fig. 3a), although these do not emerge clearly at a spatially aggregated level (Fig. S8b, c). The strongest correlations in many regions are observed at non-zero lags (Fig. 3c). Less clear patterns emerge for end of season (Fig. 3b), although there are generally negative correlations around the Mediterranean, as also reflected in the aggregated data for all but one of the landclasses in the two Mediterranean climate zones (Fig. S8f, g).

The definitions of the start of season and end of season (Sect. 2.2.2) imply that both should reflect large local EVI2 anomalies. As such, the significant EVI2–JLI correlations shown in Fig. 3a, b support anomalies in the jet's latitudinal position modulating start of season and end of season timings. We cannot directly verify this in the bi-weekly EVI2 data, because year-to-year variations in GS timing are likely shorter than two weeks for most of Europe (Chmielewski and Rötzer, 2002; Jeong et al., 2011). Nonetheless, the lagged start of season correlations underscore the importance of the pre-GS conditions for the initial phase of the GS (Fig. 3c). Such lagged effects are likely caused by multiple location-dependent mechanisms, from snow accumulation during the cold season modulating later water availability (e.g. Wang et al., 2018), to autumn and winter temperatures (e.g. Fu et al., 2012; Beil et al., 2021) or winter precipitation (Yun et al., 2018) affecting spring budburst. In Fennoscandia, England and eastern Europe, the maximum EVI2–JLI correlation pattern for the start of season (Fig. 3a) broadly matches that of the entire GS (Fig. 1a), even if the maximum correlations are mostly found at negative lags (Fig. 3c). This points to the importance of pre-GS conditions in determining the start of season and directly or indirectly affecting the entire GS. Over much of France and southern Europe, the positive correlations in Fig. 3a are not seen for the entire GS, suggesting that pre-GS lagged climate effects are important at the start of season, but are confounded by other processes during the rest of the GS. The longer GS in the more southern locations (Fig. S2d) supports this explanation.

Altogether, these results suggest that jet variability modulates GS onset, with a northward- (southward-)shifted jet bringing an earlier (later) GS start to a large part of Europe. Over several of the regions showing a positive correlation in Fig. 3a, the start of season occurs in early spring to early summer (Fig. S2a), when the JLI displays a positive correlation with temperature and radiation anomalies over much of the continent (Fig. S3a,e), and when soil moisture is typically not the dominant control on vegetation (Fig. S1d). In turn, temperature anomalies at start of season strongly and positively correlate with EVI2 across Europe (not shown, see Fig. S7a for early GS). Conversely, for end of season the widespread area of negative correlations between JLI and temperature anomalies in parts of the Mediterranean region (Fig. S3b) suggest an earlier (later) end of season there when the jet is shifted northwards (southwards). A northward-shifted jet at the end of season is associated with decreased soil moisture in much of the region, and the converse holds for a southward-shifted jet. Soil moisture is in turn the dominant control on end of season, especially where the GS ends during the summer months (not shown).

3.2. Spatio-Temporal Modulators of the Role of Jet Variability

The sign and strength of the correlation between EVI2 anomalies and JLI depend not only on the climate zone (Fig. 1, S1b) but also on the dominant landclass and GS subperiod (Fig. 4). JLI is positively correlated to EVI2 anomalies in boreal Fennoscandia (Fig. 4a), in particular during the early GS, regardless of landclass. In boreal and temperate eastern Europe, significant correlations with JLI are negative for all landclasses except DF (Fig. 4b, e). In Western Europe, the largest

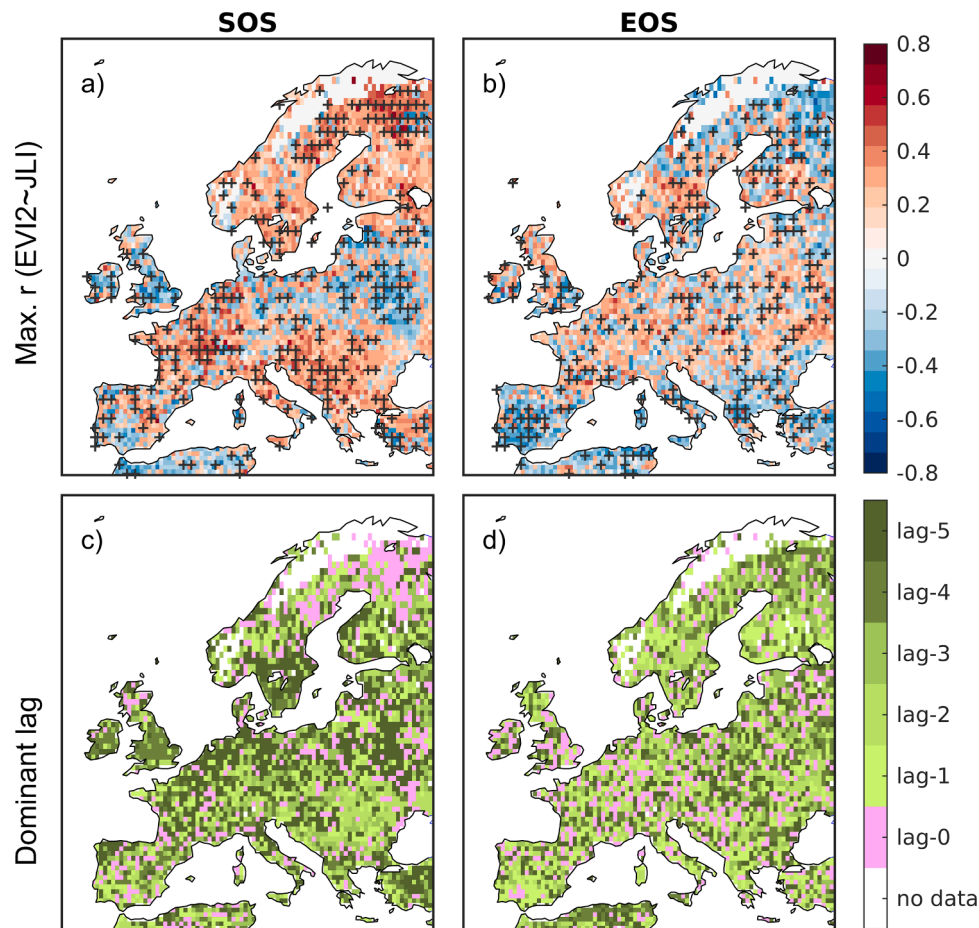


Fig. 3. (a, b) Peak GS EVI2–JLI correlation coefficients (selected based on magnitude) at lags of 0 to -5 months and (c, d) lag of peak correlation magnitude for (a, c) start of season (SOS), and (b, d) end of season (EOS). In (a, b), gridpoints with a significant correlation coefficient ($p < 0.05$) are stippled.

negative correlations are found for WS and CRP, with late GS correlations being significantly more negative than early GS ones (Fig. 4c). Finally, in the Mediterranean region JLI and EVI2 anomalies are negatively correlated, in particular for the entire GS and late GS (Fig. 4f, g).

Patterns of significant EVI2–JLI correlations are consistent across the different landclasses within each climate zone, except in eastern and central Europe. In boreal eastern Europe, DF is significantly positively correlated with JLI during the early GS, whereas the other landclasses are negatively correlated (Fig. 4b). DF is primarily located along the Carpathian range, and its high altitude makes it sensitive to temperature anomalies, which are positively correlated with JLI there (Figs. S1d, S6a). In temperate central Europe, EF and CRP have both weak but significant entire GS correlations with JLI, yet EF is positively correlated with JLI, while CRP is negatively correlated (Fig. 4d). CRP includes annual plants, which are highly dependent on soil moisture, in particular soon after establishment. EF has a well-established root system from previous years, and temperature and radiation conditions likely play a more important role.

Depending on landclass and climate zone, any of early GS, late GS or entire GS correlations can dominate. Correlations are stronger in the late than in the early GS in the Mediterranean and in some of the temperate regions and landclasses, while early GS displays the higher correlations in the boreal climates (Fig. 4). There, spring conditions are key for phenology and summer activity (Wu et al., 2021b), whereas different drivers likely combine (and confound the relation of EVI2 with JLI) during late GS: temperature and radiation (Fig. S1e, Hänninen and Tanino, 2011; Way, 2011), but also summer water availability and timing of spring phenology (Keenan and Richardson, 2015; Sade et al., 2018). Conversely, in parts of the Mediterranean region – including

Iberia and southern Italy – the bulk of the GS is outside of the canonical summer months and the end of season occurs in early to mid-summer (Fig. S2). The negative EVI2–JLI correlation in these regions mirrors the negative correlation between JLI and soil moisture anomalies during the late GS (Fig. S6f). Finally, over crop and shrubland-dominated parts of western Europe, unlike in the boreal regions, the JLI–soil moisture anomalies correlation in the late GS is stronger than the JLI–temperature anomalies correlation in the early GS (e.g. eastern England, cf. Fig. S6a, f). This results in a stronger EVI2–JLI correlation during late GS for these landclasses. Indeed, the late GS in temperate western Europe comes in late summer and autumn, when the JLI correlates negatively with soil moisture anomalies (Fig. S3 j, k) and when soil moisture is a strong and positive controlling factor in the region (Figs. S1e, S7f).

The above-discussed relative importance of early versus late GS correlations is in partial agreement with the results obtained for canonical climate modes of variability, such as the North Atlantic Oscillation and East Atlantic Pattern. The impact of these modes on EVI2 was found to be generally largest during the initial months of the GS in both the boreal and temperate climate zones, while no clear dependence on growing season subperiod emerged in the Mediterranean region (Wu et al., 2021b). We ascribe the differences between our results and those of Wu et al., (2021b) in the temperate and Mediterranean regions to the different information conveyed by the JLI relative to indices such as the North Atlantic Oscillation or East Atlantic Pattern. Indeed, the normalised indices of climate modes are often defined relative to a fixed monthly or seasonal spatial pattern in some atmospheric or oceanic variable, while the JLI continuously tracks the jet's location throughout its seasonal cycle. Taking temperate western Europe as an example, we argue that the close relationship between the JLI and late GS EVI2 is

GS-based EVI2~JLI(r) by climate zone and land class

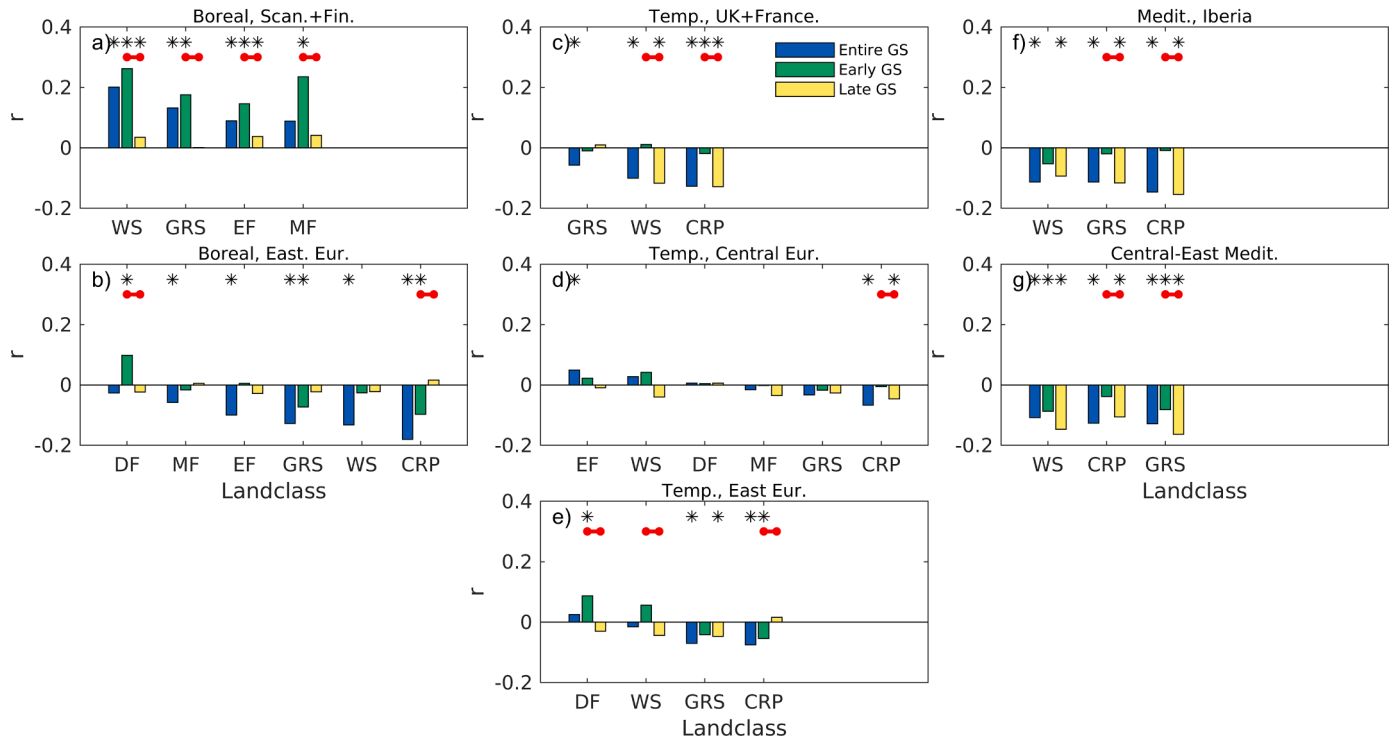


Fig. 4. Simultaneous EVI2–JLI correlation coefficients for entire, early and late GS, averaged over individual climate zones and landclasses (see Fig. S1a, b). The landclasses are ordered according to decreasing entire GS correlation values within each climate zone. Asterisks indicate significant correlations ($p < 0.05$). Red dots linked with a red line indicate significant differences between the early GS and late GS values using the two-sample Student’s t-test ($p < 0.05$).

mediated by soil moisture, whose anomalies have a variable correlation with JLI across seasons (Fig. S3i–l).

dynamics and vegetation activity. This is in spite of the potential confounding effects exerted by the pre-GS conditions, evidenced by the strong EVI2–JLI correlations lagged by a few months (Fig. S9). Similar to

The analysis thus far provides a clear link between the jet stream

Entire GS JLI and ZSI by climate zone and land class

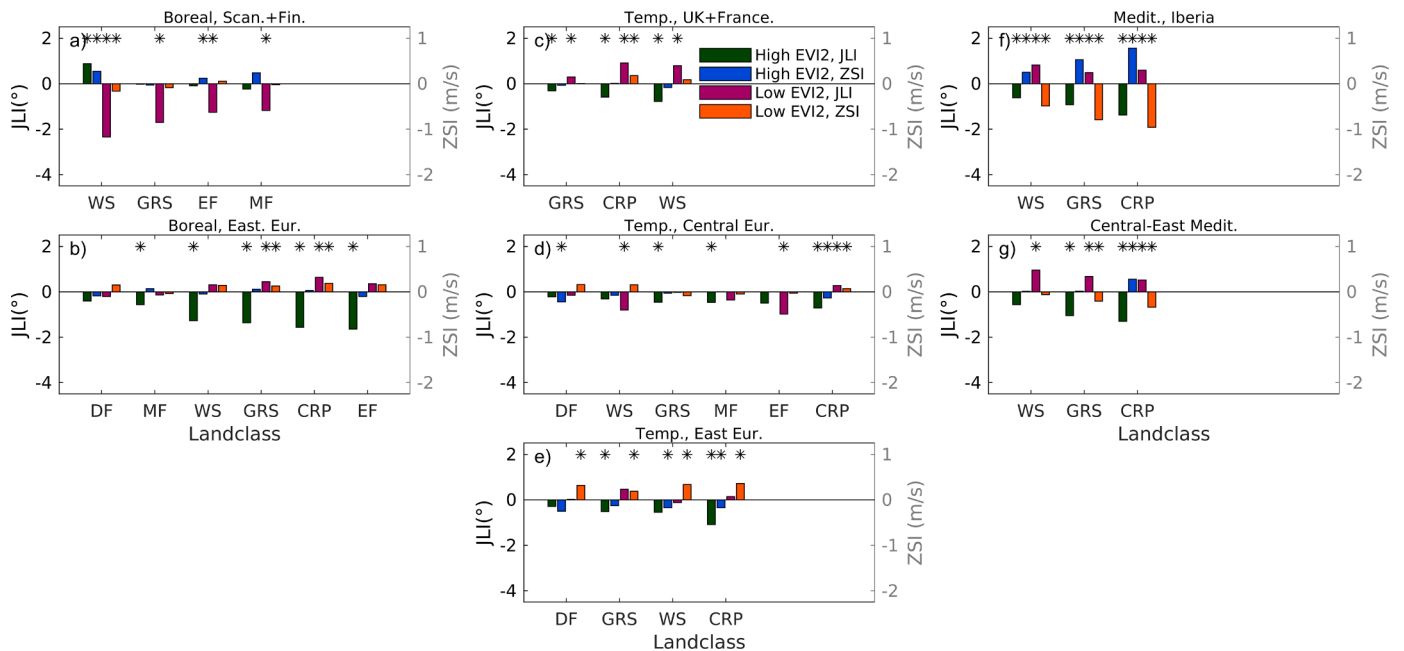


Fig. 5. JLI (degrees latitude, left-hand side axes) and ZSI ($m s^{-1}$, right-hand side axes) for anomalously high or low GS EVI2 for the same climate zones and landclasses as in Fig. 4. The ZSI is computed for the same latitudes as the individual EVI2 gridpoints considered. Dark green (purple) bars show average JLI for high (low) GS EVI2. Blue (orange) bars show average ZSI for high (low) GS EVI2. Anomalously high or low GS EVI2 are identified as entire GS in the top or bottom 10%, respectively, of the local distribution of GS-mean EVI2 anomalies. Asterisks indicate JLI or ZSI values which are significantly different from zero ($p < 0.05$).

the synchronous correlations, the lagged correlations are stronger in the late GS than in the early GS for several landclasses and climate zones. This suggests an important role of early GS or peak of season conditions in modulating late GS EVI2. In some climate zones, such as boreal eastern Europe, allowing for lags in the EVI2–JLI correlation actually shifts the relative strengths of early GS versus late GS correlations (cf. Figs. 4b, S9b). However, in many other zones and landclasses the lagged correlations of EVI2 anomalies with the JLI tend to be relatively stationary on timescales of 1–2 months (cf. Fig. 4, S9), pointing to robust JLI impacts on vegetation. The variability of correlation with lag is larger for climate modes of variability (Wu et al., 2021b; note that they aggregated results over different geographical areas than those used here), again pointing to the complementarity of the jet and climate mode analyses.

Composites of JLI conditioned on GS with locally anomalously high or low EVI2 values (Fig. 5), reflect the EVI2–JLI correlations. In other words, many landclass–climate zone combinations that display significant EVI2–JLI correlations also show large absolute JLI values when compositing on anomalously high or low GS EVI2. In boreal Fennoscandia, anomalously low GS EVI2 correspond to significant negative JLI values for all landclasses (Fig. 5a). In this region in general EVI2–JLI correlations are strongly positive (Fig. 4a), and the southward-shifted jet during anomalously low GS EVI2 reflects a cooler early GS in the region (Fig. S6a). Boreal eastern Europe and the temperate and Mediterranean regions also show a close match between EVI2–JLI correlations and JLI values for anomalously high or low GS EVI2 (cf. Figs. 4b–g, 5b–g). For example, boreal eastern Europe displays significant negative JLI values during anomalously high GS EVI2 (Fig. 5b). The only exception is DF, which is also the only landclass in the region not displaying a significant entire GS EVI2–JLI correlation.

We complement the picture provided by the JLI by analysing the ZSI. The latter does not track a dynamical feature of the atmosphere as done by the JLI, but instead measures anomalies in the zonal flow at a fixed latitude. It therefore provides information on the relation between climate zone, windspeed, landclass position and GS EVI2 in an absolute sense, as opposed to relative to the location of the jet stream. As done for the JLI, we test whether large anomalies in EVI2 correspond to large ZSI values. This would mean that zonal flow variability at a given latitude has a physical footprint on vegetation greenness at such latitude, supporting the relevance of dynamical atmospheric indicators for the study of vegetation activity in Europe.

In general, the ZSI and JLI composites are consistent with one another, although the largest composite values occur in different climate zones and geographical regions. In temperate eastern Europe, anomalously low GS EVI2 correspond to significant positive ZSI for all landclasses, while only GRS and CRP for anomalously high EVI2 show a significant signal in JLI (Fig. 5e). Since this region is relatively far from the Atlantic, the influence of the jet is likely dictated by how far the zonal flow extends over the continent, and latitudinal jet shifts with weak zonal winds play little role. The largest speed anomalies are observed in the Mediterranean region, where there is a close match between anomalously high GS EVI2 and positive speed anomalies and anomalously low GS EVI2 and negative speed anomalies (Fig. 5f, g). The large magnitude of the ZSI composites may partly be ascribed to the climatologically stronger large-scale zonal atmospheric flow – and hence larger variability in absolute terms – during spring and autumn than during summer (e.g. Koch et al., 2006). The GS in much of the Mediterranean region spans all these meteorological seasons, while in most of the rest of Europe only parts of spring and autumn are included (Fig. S2). Combining this information with that from the JLI, the picture in the Mediterranean region is of a southward-shifted, fast-flowing jet during anomalously high GS EVI2, and a northward-shifted, slow jet during anomalously low GS EVI2. It is indeed the case that a southward-shifted jet tends to be intense, zonally extended and exit over the western Mediterranean during spring, summer and autumn (Fig. S4e–g). This jet configuration favours the inflow of moist oceanic air to the region especially during spring and autumn, when compared to a

northward-shifted jet (Fig. S5 e,g). We conclude that the variability of jet and zonal flow indices can be mapped to large-scale anomalies in both the atmospheric circulation and vegetation greenness in Europe. This supports the JLI correlations discussed above having a clear physical footprint.

4. Further discussion and conclusions

The European vegetation activity and climate variability are closely connected by feedback loops and two-way interactions (see Introduction). Here, we focussed on how climate variability may control vegetation activity across the continent. We showed that jet stream variability can help to understand this complex link by relating canonical drivers of vegetation activity to large-scale atmospheric dynamics, and effectively explains regional EVI2 anomalies over large parts of Europe. We have specifically related remotely-sensed vegetation greenness (EVI2) to an index related to the meridional location of the North Atlantic jet (JLI) and one related to zonal windspeed across the North Atlantic and Europe (ZSI). These two indices are grounded in the large-scale dynamics of the atmosphere. Unlike commonly used indices of climate modes of variability, they do not rely on projections of climate variables on fixed spatial patterns or decomposition in orthogonal modes.

The correlation of EVI2 anomalies with the JLI points to a significant control of the jet latitude on growing season (GS) conditions over large parts of Europe, mediated by the specific factor(s) governing vegetation greenness in each region. Indeed, the JLI shows regionally significant correlations with temperature, soil moisture and downward surface solar radiation anomalies throughout the year, with patterns changing seasonally due to differing climatological conditions. Almost the whole of Fennoscandia – a region mostly controlled by temperature and radiation – shows a positive correlation between GS greenness anomalies and jet latitude anomalies. Conversely, the same correlation is predominantly negative in eastern Europe, reflecting the combined effect of radiation and soil moisture anomalies there. The role of the jet in modulating vegetation greenness across landclasses and climate zones highlights a rich variety of local features. Jet stream variability can also modulate the onset and end of the GS across Europe. The correlations between EVI2 anomalies and the jet and zonal flow indices have a clear physical footprint, as apparent when conditioning JLI and ZSI on locally anomalously high or low GS greenness. We argue that this supports a causal relationship between jet variability and anomalies in vegetation activity. As a caveat, our correlation analysis is unable to distinguish the relative importance of southwards versus northwards shifts of the jet, except for the analysis focusing on the anomalously high or low GS greenness. Moreover, a rigorous proof of causation would require a more detailed statistical investigation, and a mechanistic understanding of the vegetation-based processes explaining the greenness response to jet variability.

Differently from previous studies based on fixed-month GS, we considered a locally-defined GS. This enables us to focus on the months relevant to local vegetation activity and directly compare the vegetation–climate coupling for different land-cover types at a specific GS stage. For example, the climate anomalies associated with a meridional excursion of the jet in late July – the peak growing period over much of Scandinavia – are radically different from those in winter – the core GS over the warmer parts of the Mediterranean region (Figs. S2, S3). The use of a single set of GS months would confound this signal, and we argue that a locally-defined GS provides additional insights into the atmospheric controls on regional vegetation greenness (e.g. c.f. Fig. 3 in Gonsamo et al. (2016), based on a fixed-months GS with Fig. 5 in Wu et al. (2021b)), based on a locally-defined GS). We further divide the GS into two subperiods: early GS and late GS. In agreement with Wu et al. (2021b), we find a differential contribution of these two subperiods to the climate–vegetation coupling in Europe.

The emerging strong relationship between jet stream variability and

vegetation greenness has implications at multiple timescales. The significant correlations between JLI and EVI2 anomalies at lags of several months are potentially relevant in a sub-seasonal to seasonal vegetation predictability perspective. Indeed, variations in jet latitude are a key source of seasonal predictability in the Euro-Atlantic sector (Parker et al., 2019). The jet can also display extreme anomalies on seasonal scales (e.g. Santos et al., 2013). The impacts of persistent jet anomalies on vegetation are yet to be investigated. In a long-term variability and climate change context, historical data and reconstructions show that the jet stream displays significant interdecadal variability (e.g. Woolings et al., 2014). Climate model simulations further produce a poleward shift of the jet and an enhanced jet speed seasonal cycle under greenhouse forcing (Stendhel et al., 2021, and references therein), although the physical mechanisms underlying these changes are debated (Shaw, 2019). The study of jet–vegetation interactions, including both jet location and large-scale zonal windspeed, can thus provide a lens to relate dynamical changes and variability of the atmospheric circulation to impacts on vegetation activity.

Declaration of Competing Interest

The authors declare that they have no known competing financial interests or personal relationships that could have appeared to influence the work reported in this paper.

Acknowledgments

G. Messori, M. Wu and G. Vico acknowledge the support of the Swedish Research Council FORMAS (Grant No. 2018-00968). G. Messori additionally acknowledges funding from the European Research Council (ERC) under the European Union's Horizon 2020 research and innovation programme (Grant agreement No. 948309, CENÆ Project). G. Vico additionally acknowledges the European Commission and the Swedish Research Council FORMAS (Grant No. 2018-02787) for funding in the frame of the collaborative international consortium iAquaduct financed under the 2018 Joint call of the WaterWorks 2017 ERA-NET Cofund. This ERA-NET is an integral part of the activities developed by the Water JPI. M. Galfi acknowledges the support of the Air, Water and Landscape Science research programme at the Dept. of Earth Sciences, Uppsala University. All authors would like to thank S. Manzoni and two anonymous reviewers for constructive feedback on the manuscript.

Supplementary materials

Supplementary material associated with this article can be found, in the online version, at [doi:10.1016/j.agrformet.2022.109008](https://doi.org/10.1016/j.agrformet.2022.109008).

References

- Bastos, A., Orth, R., Reichstein, M., Ciais, P., Viovy, N., Zaehle, S., Sitch, S., 2021. Vulnerability of European ecosystems to two compound dry and hot summers in 2018 and 2019. *Earth Syst. Dyn.* 12 (4), 1015–1035.
- Belmecheri, S., Babst, F., Hudson, A. R., Betancourt, J., Trouet, V., 2017. Northern hemisphere jet stream position indices as diagnostic tools for climate and ecosystem dynamics. *Earth Interact.* 21, 1–23.
- Beil, I., Kreyling, J., Meyer, C., Lemcke, N., Malyshev, A. V., 2021. Late to bed, late to rise-warmer autumn temperatures delay spring phenology by delaying dormancy. *Glob. Change Biol.* 27, 5806–5817 in press.
- Bjerknes, J., 1969. Atmospheric teleconnections from the equatorial Pacific. *Mon. Weather Rev.* 97, 163–172.
- Chmielewski, F.M., Rötzer, T., 2002. Annual and spatial variability of the beginning of growing season in Europe in relation to air temperature changes. *Clim. Res.* 19 (3), 257–264.
- Dommenget, D., Latif, M., 2002. A cautionary note on the interpretation of EOFs. *J. Clim.* 15 (2), 216–225.
- Faranda, D., Sato, Y., Messori, G., Moloney, N.R., Yiou, P., 2019. Minimal dynamical systems model of the Northern Hemisphere jet stream via embedding of climate data. *Earth Syst. Dynam.* 10, 555–567. <https://doi.org/10.5194/esd-10-555-2019>.
- Friedl, M.A., Sulla-Menashe, D., Tan, B., Schneider, A., Ramankutty, N., Sibley, A., Huang, X., 2010. MODIS Collection 5 global land cover: Algorithm refinements and characterization of new datasets. *Remote Sens. Environ.* 114 (1), 168–182.
- Fu, Y.H., Campioli, M., Deckmyn, G., Janssens, I.A., 2012. The impact of winter and spring temperatures on temperate tree budburst dates: results from an experimental climate manipulation. *PLoS One*. <https://doi.org/10.1371/journal.pone.0047324>.
- Gaetani, M., Baldi, M., Dalu, G.A., Maracchi, G., 2011. Jetstream and rainfall distribution in the Mediterranean region. *Nat. Hazards Earth Syst. Sci.* 11 (9), 2469–2481.
- Glantz, M.H., Katz, R.W., Nicholls, N., 1991. *Teleconnections Linking Worldwide Climate Anomalies*, 535. Cambridge University Press, Cambridge.
- Gonsamo, A., Chen, J.M., Lombardozzi, D., 2016. Global vegetation productivity response to climatic oscillations during the satellite era. *Glob. Change Biol.* 22 (10), 3414–3426.
- Gouveia, C., Trigo, R.M., DaCamara, C.C., Libonati, R., Pereira, J., 2008. The North Atlantic oscillation and European vegetation dynamics. *Int. J. Climatol.* 28, 1835–1847.
- Gouveia, C.M., Trigo, R.M., Beguería, S., Vicente-Serrano, S.M., 2017. Drought impacts on vegetation activity in the Mediterranean region: An assessment using remote sensing data and multi-scale drought indicators. *Glob. Plan. Change* 151, 15–27.
- Harnik, N., Galanti, E., Martius, O., Adam, O., 2014. The anomalous merging of the African and North Atlantic jet streams during the Northern Hemisphere winter of 2010. *J. Clim.* 27 (19), 7319–7334.
- Held, I.M., 1975. Momentum transport by quasi-geostrophic eddies. *J. Atmos. Sci.* 32, 1494–1497.
- Held, I.M., Hou, A.Y., 1980. Nonlinear axially symmetric circulations in a nearly inviscid atmosphere. *J. Atmos. Sci.* 37, 515–533.
- Hersbach, H., Bell, B., Berrisford, P., Hirahara, S., Horányi, A., Muñoz-Sabater, J., Thépaut, J.N., 2020. The ERA5 global reanalysis. *Q. J. R. Met. Soc.* 146 (730), 1999–2049.
- Hudson, A.R., Alfaro-Sanchez, R., Babst, F., Belmecheri, S., Moore, D.J., Trouet, V., 2019. Seasonal and synoptic climatic drivers of tree growth in the Bighorn Mountains, WY, USA (1654–1983 CE). *Dendrochronologia* 58, 125633.
- Hurrell, J.W., Kushnir, Y., Visbeck, M., 2001. The north Atlantic oscillation. *Science* 291, 603–605.
- Hänninen, H., Tanino, K., 2011. Tree seasonality in a warming climate. *Trends Plant Sci.* 16 (8), 412–416.
- Jeong, S.J., HO, C.H., GIM, H.J., Brown, M.E., 2011. Phenology shifts at start vs. end of growing season in temperate vegetation over the Northern Hemisphere for the period 1982–2008. *Glob. Change Biol.* 17 (7), 2385–2399.
- Jiang, Z., Huete, A.R., Didan, K., Miura, T., 2008. Development of a two-band enhanced vegetation index without a blue band. *Remote Sens. Environ.* 112 (10), 3833–3845.
- Jiang, B., Liang, S., Yuan, W., 2015. Observational evidence for impacts of vegetation change on local surface climate over northern China using the Granger causality test. *J. Geophys. Res. Biogeosci.* 120, 1–12. <https://doi.org/10.1002/2014JG002741>.
- Jones, C.D., Collins, M., Cox, P.M., Spall, S.A., 2001. The carbon cycle response to ENSO: a coupled climate-carbon cycle model study. *J. Clim.* 14 (21), 4113–4129.
- Keenan, T.F., Richardson, A.D., 2015. The timing of autumn senescence is affected by the timing of spring phenology: Implications for predictive models. *Glob. Change Biol.* 21 (7), 2634–2641.
- Koch, P., Wernli, H., Davies, H.C., 2006. An event-based jet-stream climatology and typology. *Int. J. Clim.* 26 (3), 283–301.
- Kottek, M., Grieser, J., Beck, C., Rudolf, B., Rubel, F., 2006. World Map of the Köppen-Geiger climate classification updated. *Meteorol. Zeits.* 15 (3), 259–263.
- Marquis, B., Bergeron, Y., Simard, M., Tremblay, F., 2020. Probability of spring frosts, not growing degree-days, drives onset of spruce bud burst in plantations at the boreal-temperate forest ecotone. *Front. Plant Sci.* 11, 1031.
- Martens, B., Miralles, D.G., Lievens, H., van der Schalie, R., de Jeu, R.A.M., Fernández-Prieto, D., et al., 2017. GLEAM v3: satellite-based land evaporation and root-zone soil moisture. *Geosci. Mod. Dev.* 10 (5), 1903–1925. <https://doi.org/10.5194/gmd-10-1903-2017>.
- Miralles, D.G., Holmes, T.R.H., De Jeu, R.A.M., Gash, J.H., Meesters, A.G.C.A., Dolman, A.J., 2011. Global land-surface evaporation estimated from satellite-based observations. *Hydr. Earth Syst. Sci.* 15 (2), 453–469. <https://doi.org/10.5194/hess-15-453-2011>.
- Meng, X.H., Evans, J.P., McCabe, M.F., 2014. The impact of observed vegetation changes on land-atmosphere feedbacks during drought. *J. Hydrometeorol.* 15 (2), 759–776.
- Menzel, A., Yuan, Y., Matiu, M., Sparks, T., Scheifinger, H., Gehrig, R., Estrella, N., 2020. Climate change fingerprints in recent European plant phenology. *Glob. Change Biol.* 26 (4), 2599–2612.
- Messori, G., Caballero, R., 2015. On double Rossby wave breaking in the North Atlantic. *J. Geophys. Res.: Atmos.* 120 (21), 11–129.
- Messori, G., Caballero, R., Gaetani, M., 2016. On cold spells in North America and storminess in western Europe. *Geophys. Res. Lett.* 43 (12), 6620–6628.
- Messori, G., Ruiz-Pérez, G., Manzoni, S., Vico, G., 2019. Climate drivers of the terrestrial carbon cycle variability in Europe. *Environ. Res. Lett.* 14 (6), 063001 <https://doi.org/10.1088/1748-9326/ab1ac0>.
- Messori, G., Harnik, N., Madonna, E., Lachmy, O., Faranda, D., 2021. A dynamical systems characterization of atmospheric jet regimes. *Earth Syst. Dyn.* 12 (1), 233–251.
- Molnos, S., MAMDOUTH, T., Petri, S., Nocke, T., Weinkauff, T., Coumou, D., 2017. A network-based detection scheme for the jet stream core. *Earth Syst. Dyn.* 8 (1), 75–89.
- Muffler, L., Beierkuhnlein, C., Aas, G., Jentsch, A., Schweiger, A.H., Zohner, C., Kreyling, J., 2016. Distribution ranges and spring phenology explain late frost sensitivity in 170 woody plants from the Northern Hemisphere. *Glob. Ecol. Biogeogr.* 25 (9), 1061–1071.

- Öquist, G., Huner, N.P.A., 2003. Photosynthesis of overwintering evergreen plants. *Ann. Rev. Plant Biol.* 54 (1), 329–355.
- Parker, T., Woollings, T., Weisheimer, A., O'Reilly, C., Baker, L., Shaffrey, L., 2019. Seasonal predictability of the winter North Atlantic Oscillation from a jet stream perspective. *Geophys. Res. Lett.* 46 (16), 10159–10167.
- Rosby, C.G., 1947. On the distribution of angular velocity in gaseous envelopes under the influence of large-scale horizontal mixing processes. *Bull. Amer. Meteorol. Soc.* 28 (2), 53–68.
- Rödenbeck, C., Zaehle, S., Keeling, R., Heimann, M., 2018. How does the terrestrial carbon exchange respond to inter-annual climatic variations? A quantification based on atmospheric CO₂ data. *Biogeosciences* 15, 2481–2498. <https://doi.org/10.5194/bg-15-2481-2018>.
- Röthlisberger, M., Pfahl, S., Martius, O., 2016. Regional-scale jet waviness modulates the occurrence of midlatitude weather extremes. *Geophys. Res. Lett.* 43 (20), 10–989.
- Sade, N., Del Mar Rubio-Wilhelmi, M., Umnajkitikorn, K., Blumwald, E., 2018. Stress-induced senescence and plant tolerance to abiotic stress. *J. Exp. Bot.* 69 (4), 845–853.
- Santos, J.A., Woollings, T., Pinto, J.G., 2013. Are the winters 2010 and 2012 archetypes exhibiting extreme opposite behavior of the North Atlantic jet stream? *Mon. Weather Rev.* 141 (10), 3626–3640.
- Shaw, T.A., 2019. Mechanisms of future predicted changes in the zonal mean mid-latitude circulation. *Curr. Clim. Change Rep.* 5 (4), 345–357.
- Stendel, M., Francis, J., White, R., Williams, P.D., Woollings, T., 2021. The jet stream and climate change. *Climate Change*. Elsevier, pp. 327–357.
- Urbanski, S., Barford, C., Wofsy, S., Kucharik, C., Pyle, E., Budney, J., McKain, K., Fitzjarrald, D., Czirkowsky, M., Munger, J.W., 2007. Factors controlling CO₂ exchange on timescales from hourly to decadal at Harvard Forest. *J. Geophys. Res.* 112, G02020.
- Yun, J., Jeong, S.-J., Ho, C.-H., Park, C.-E., Park, H., Kim, J., 2018. Influence of winter precipitation on spring phenology in boreal forests. *Glob. Change Biol.* 24, 5176–5187.
- Wang, J., Rich, P.M., Price, K.P., 2003. Temporal responses of NDVI to precipitation and temperature in the central Great Plains, USA. *Int. J. Remote Sens.* 24 (11), 2345–2364.
- Wang, T., Ciais, P., Piao, S.L., Ottlé, C., Brender, P., Maignan, F., Verma, S., 2011. Controls on winter ecosystem respiration in temperate and boreal ecosystems. *Biogeosciences* 8, 2009–2025.
- Wang, X., Wang, T., Guo, H., Liu, D., Zhao, Y., Zhang, T., Piao, S., 2018. Disentangling the mechanisms behind winter snow impact on vegetation activity in northern ecosystems. *Glob. Change Biol.* 24 (4), 1651–1662.
- Way, D.A., 2011. Tree phenology responses to warming: spring forward, fall back? *Tree Physiol.* 31 (5), 469–471.
- Williams, I.N., Torn, M.S., 2015. Vegetation controls on surface heat flux partitioning, and land-atmosphere coupling. *Geophys. Res. Lett.* 42, 9416–9424. <https://doi.org/10.1002/2015GL066305>.
- Woollings, T., Hannachi, A., Hoskins, B., 2010. Variability of the North Atlantic eddy-driven jet stream. *Q. J. R. Met. Soc.* 136 (649), 856–868.
- Woollings, T., Czuchnicki, C., Franzke, C., 2014. Twentieth century North Atlantic jet variability. *Q. J. Roy. Met. Soc.* 140 (680), 783–791.
- Wu, M., Schurgers, G., Ahlström, A., Rummukainen, M., Miller, P.A., Smith, B., May, W., 2017. Impacts of land use on climate and ecosystem productivity over the Amazon and the South American continent. *Environ. Res. Lett.* 12 (5), 054016.
- Wu, M., Smith, B., Schurgers, G., Ahlström, A., Rummukainen, M., 2021a. Vegetation-climate feedbacks enhance spatial heterogeneity of Pan-Amazonian ecosystem states under climate change. *Geophys. Res. Lett.* 48 (8) e2020GL092001.
- Wu, M., Vico, G., Manzoni, S., Cai, Z., Bassiouni, M., Tian, F., et al., 2021b. Early growing season anomalies in vegetation activity determine the large-scale climate-vegetation coupling in Europe. *J. Geophys. Res.: Biogeosci.* 126 <https://doi.org/10.1029/2020JG006167> e2020JG006167.
- Zeng, N., Neelin, J.D., 2000. The role of vegetation-climate interaction and interannual variability in shaping the African savanna. *J. Clim.* 13 (15), 2665–2670.
- Zeng, Z., Piao, S., Li, L., 2017. Climate mitigation from vegetation biophysical feedbacks during the past three decades. *Nature Clim. Change* 7, 432–436. <https://doi.org/10.1038/nclimate3299>.
- Zhu, Z., Piao, S., Myneni, R.B., Huang, M., Zeng, Z., Canadell, J.G., Zeng, N., 2016. Greening of the Earth and its drivers. *Nature Clim. Change* 6 (8), 791–795.